Merged Statistical Analyses of Historical Monthly Precipitation Anomalies Beginning 1900

Thomas M. Smith[1], Phillip A. Arkin[2], Mathew R.P. Sapiano[2], Ching-Yee Chang[3]

1. NOAA/STAR/SCSB and CICS/ESSIC, 5825 Univ. Research Ct., Suite 4001, College Park, MD, 20740
2. Univ. Maryland, CICS/ESSIC, 5825 Univ. Research Ct., Suite 4001, College Park, MD, 20740
3. Univ. California, Dept. of Geography, 595 McCone Hall, Berkeley, CA 94720

October 23, 2009

To be submitted to *J. Climate*

ABSTRACT

A monthly reconstruction of precipitation beginning 1900 is presented. The reconstruction is intended to resolve interannual and longer time scales and spatial scales larger than 5º over both land and oceans. Because of different land and ocean data availability, the reconstruction is produced by combining two separate historical reconstructions. One analyzes interannual time-scale variations directly by fitting gauge-based anomalies to large-scale spatial modes. That direct reconstruction is used for land anomalies and interannual oceanic anomalies. The other analyzes annual and longer time-scale variations indirectly from correlations with analyzed sea-surface temperature and sea-level pressure. The indirect reconstruction is used for oceanic variations with time scales longer than interannual. In addition to the reconstruction, a method of estimating reconstruction errors is also presented.

Over land the reconstruction is a filtered representation of the gauge data with data gaps filled. Over oceans the reconstruction gives an estimate of the atmospheric response to changing temperature and pressure, combined with interannual variations. The reconstruction makes it possible to evaluate global precipitation variations for time periods much longer than the satellite period, which begins 1979. Evaluations of the reconstruction show some large-scale similarities with coupled model precipitation variations over the 20th century, including an increasing tendency over the century. The reconstruction land and sea trends tend to be out of phase at low latitudes, similar to the out-of-phase relationship for interannual variations. The reconstruction presented here may be used for climate monitoring, statistical climate studies of the 20th century, and for helping to evaluate dynamic climate models. In the future we will explore the possibility of improving the reconstruction by including other data that may give independent information about the precipitation history.

1. Introduction

Observations from a number of earth-orbiting satellites combined with rain gauge measurements make it possible to analyze global precipitation for the satellite era. Monthly precipitation analyses beginning in 1979 have been produced by the Global Precipitation Climatology Project (GPCP, Huffman *et al.* 1997, Adler *et al.* 2003, Huffman *et al.* 2009) and Xie and Arkin (CMAP, 1996, 1997). These land-ocean analyses are valuable for assessing global and regional climate variability in the satellite era. For climate-change studies it is desirable to have longer records. Here we discuss improved methods for using the available historical observations with statistics obtained from satellite-based data to extend the global precipitation record back to 1900. This includes ocean-area precipitation, an important component of the global hydrologic cycle which could be affected by climate change.

Over the oceans both sea-surface temperature (SST) and sea-level pressure (SLP) have been reconstructed through the 20th century (*e.g.*, see Smith *et al.* 2005, 2008a, and Allan and Ansell 2006). Oceanic monthly reconstructions of SST and SLP anomalies are possible because they were regularly measured by ships over the 20th century (*e.g.*, Woodruff *et al.* 1998) and because of their relatively large time and space scales. The longer climate records allow SST and SLP reconstructions to be used to better understand climate variations and to validate climate models. Historical precipitation beginning 1900 is available for many land regions from rain gauge measurements (*e.g.*, Vose *et al.* 1998). However, there are many land regions where gauges are sparse, and over oceans there are no systematic gauge observations for the pre-satellite period.

Reconstructions of historical precipitation that includes oceanic regions have been developed in an attempt to fill in these missing regions for the pre-satellite era. Xie *et al.* (2001) fit gauge data to a set of empirical orthogonal functions (EOFs) to reconstruct precipitation for the second half of the 20th century. Their reconstruction yielded good skill in the tropical Pacific because of its ability to reconstruct variations associated with ENSO. In most other regions their reconstruction had little skill. A similar reconstruction by Efthymiadis *et al.* (2005) gave similar results, with little skill outside the tropics except near gauge locations. Smith *et al.* (2008b) produced a similar reconstruction for monthly precipitation beginning 1900. This reconstruction, computed by fitting GHCN (Vose *et al.* 1998) gauge data to a set of EOFs, will be referred to as REOF. The REOF was based on an improved satellite base analysis and carefully tuned. Besides having high skill in the tropics, consistent with earlier studies, the REOF was found to have improved skill over Northern Hemisphere extra-tropical oceans. The REOF skill is lowest in the extra-tropical southern ocean. Another deficiency with the REOF is its multi-decadal component, which was found to be sensitive to the gauge data set used for the reconstruction. Evaluation of multi-decadal variations is important for understanding 20th century climate variations, so something more than the REOF was needed.

In an attempt to better resolve multi-decadal variations, we developed a canonical correlation analysis (CCA) relating fields of SST and SLP anomalies to precipitation anomalies (Smith *et al.* 2009, also see Barnett and Preisendorfer 1987 for a description of CCA). The SST and SLP anomalies, which are better sampled historically than precipitation and have been reconstructed over oceanic regions. Relationships for the CCA are developed using a satellite-based precipitation analysis over the satellite era. Since this reconstruction was intended to resolve large-scale multi-decadal variations, annual precipitation anomalies were analyzed using their relationships to annual SST and SLP anomalies. We will refer to this reconstruction as RCCA.

Large-scale averages of the RCCA were found to compare well with the available data. The near-global average at gauge locations is consistent with averages of independent gauges. Over oceans both the RCCA and an ensemble of AR4 coupled models (Randall *et al.* 2007) indicate increasing average precipitation on multi-decadal time scales, although the RCCA increase is stronger than that from the AR4 ensemble (see Smith *et al.* 2009 for details). However, smaller-scale variations in the RCCA are much weaker than in the REOF.

Clearly, it is desirable to blend these two analyses retaining the best features of each. The REOF has more reliable month-to-month variations and better spatial resolution, so its high-frequency variations should be part of the blended analysis. The RCCA has more reliable multi-decadal variations, so its low-frequency variations should be part of the blended analysis. In the following sections the input data and individual reconstructions to be blended are described in greater detail. Blending methods are then presented, followed by discussions of results and a summary.

2. Input Data and Reconstructions

Here we describe the different data sets needed to compute the reconstructions. Data used for comparisons with the reconstruction are also described. That is followed by a description of the reconstruction based on fitting gauge data to EOFs (REOF) and the reconstruction based on a CCA (RCCA). For both the REOF and RCCA, cross-validation tests used to tune the reconstructions and the skill of the individual analyses are discussed.

2.1 Input Data

Several satellite-based data sets are used for development of the reconstructions and also to help validate the analyses. These base data sets are needed to develop the large-scale spatial covariance patterns used to produce the reconstructions. Therefore, it is critical that they be as accurate and unbiased as possible to avoid introducing false signals to the historical reconstruction.

One satellite-based analysis used to test and to help validate the analyses is the GPCP, mentioned above (Huffman *et al.* 1997, Adler *et al.* 2003). The current version of GPCP is version 2.1 (GPCP.v2.1), which was recently released (Huffman *et al.* 2009). The GPCP combines several different infrared and microwave based satellite precipitation analyses after adjusting them to remove inter-satellite biases. The combined satellite product is merged with a gauge product. The result is a global monthly precipitation analysis on a 2.5° latitude-longitude grid beginning January 1979. Changes incorporated in GPCP.v2.1 include the use of improved gauge data from the Global Precipitation Climatology Center (GPCC) and improved adjustments for the satellite inputs. Here the GPCP.v2.1 monthly data are used from 1979-2008 for reconstruction model development and evaluation.

The statistical reconstruction models used here will use covariance computed from the satellite base period data, beginning 1979, to reconstruct the pre-satellite period, beginning 1900. Thus, it is important that the satellite period base analysis be as free from non-physical variations as possible, to prevent producing spurious reconstruction covariance. One potential problem that we considered is inhomogeneities in the data from using satellites with different sampling times and different instruments. The GPCP data have been carefully constructed for climate studies, including adjustments of inter-satellite biases. Testing on an earlier version of GPCP showed no apparent long-term biases from using multiple satellite inputs (Smith *et al.* 2006), so most if not all inhomogeneities should have been removed from GPCP. Some additional testing was done to determine if a simpler and perhaps more homogeneous satellite-period analysis could be developed similar to the analysis of Sapiano *et al.* (2008). Testing involved using satellite infrared-based precipitation estimates with homogeneity adjustments to account for time-of-day differences, combined with ERA-40 and ERA-interim reanalysis estimates. The satellite estimates were used at low latitudes and the ERA reanalysis estimates at high latitudes, with blending in between (see Sapiano *et al.* 2008 for details). Testing has shown that at this time we are not able to produce a more homogeneous satellite-period analysis using these methods. Therefore, here we use GPCP.v2.1 as base data in all of our reconstructions.

Gauge-based precipitation analyses are used for the REOF. Here several gauge analyses are tested with the REOF. All of these data sets are available online. One gauge-based analysis the Global Historical Climatology Network (GHCN, Vose *et al.* 1998), produced by the National Climatic Data Center. The GHCN is a monthly analysis on a 5º spatial grid, 1900-2008. These are the same gauge data used for reconstruction by Smith *et al.* (2008b), except that here the GHCN is updated with several more years. The Global Precipitation Climatology Center (GPCC) version 4 gauge data are also used to test our reconstructions. The monthly GPCC data are available 1901-2007. Descriptions of GPCC are given by Schneider *et al.* (2008) and Rudolf (2005). Here we average their 2.5° data to the 5° grid. In addition we also use the University of East Anglia Climate Research Unit (CRU) 5° monthly gauge analysis (Hulme *et al.* 1998). The monthly CRU analysis is available 1900 to 1998.

All three gauge-based data sets are applied to the REOF analysis. Differences can occur because of different data included in the gauge analyses, differences in gauge adjustments and quality control, and differences in averaging from individual stations to 5° regions. Gauge sampling differences are illustrated by Figure 1. For most of the historical period the CRU analysis has better sampling of 5º areas than either of the others, while GHCN has the least sampling. This figure illustrates regional coverage with at least one gauge in a 5º area, and not the total number of gauges. Thus, although the CRU has generally best spatial coverage, it may not use the greatest total number of gauges. Averaging more gauges in a 5º area will decrease the random error for that area. However, as we discuss below, the analysis involves fitting data to spatial modes, which filters out nearly all random errors. For our analysis the spatial coverage is most critical. Note that although the Earth's surface is land over approximately 30%, coastal and island 5° regions in the analyses are here assumed to cover the entire 5° area, and thus the region sampled can exceed 30% in this estimate.

As noted above, both SST and SLP historical analyses are used to in the RCCA. The SSTs are from the analysis of Smith *et al.* (2008a) and the SLPs are from the analysis of Allan and Ansell (2006). Since the RCCA is performed on an annual 5° latitude-longitude grid, those analyses are averaged to match that grid.

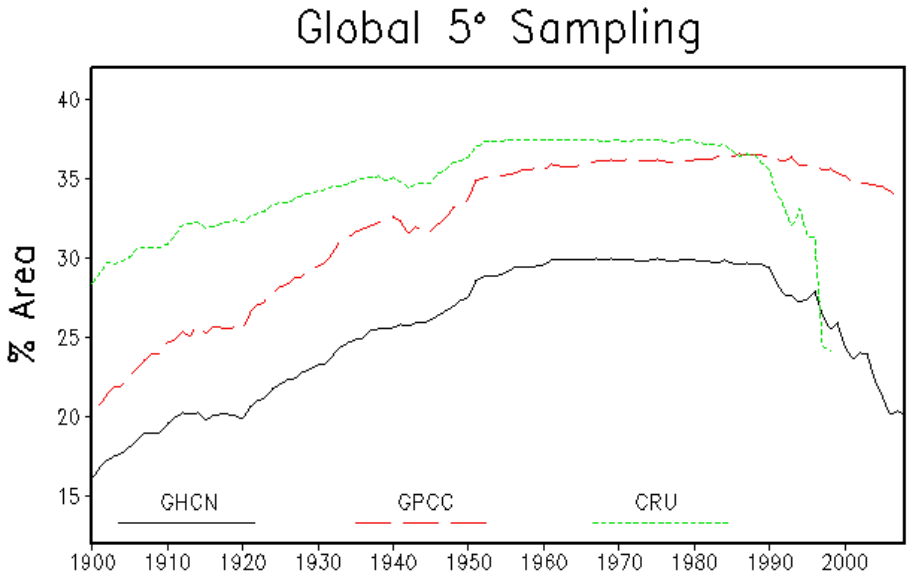

Figure 1. The % of global 5° areas sampled by each of the gauge analyses used. Annual averages of the monthly percentage of global area sampled are shown.

2.2 REOF

The method used for producing the reconstruction based on EOFs (REOF) was described by Smith *et al.* (2008b). Here we summarize the method and note differences

in the present compared to Smith *et al.* (2008b), which should be consulted for more details of the method.

The REOF analysis is developed using a set of large-scale covariance EOFs of precipitation anomalies. The EOFs need to represent spatial scales that extend from regions where data are available to all other regions. For the precipitation anomalies the only data used in the REOF is gauge data from over land and islands. We use these data to reconstruct precipitation over oceanic regions, so only the EOFs representing the largest scales are suitable for use. In addition, the REOF analysis is performed separately in three regions: 80°S-20°S, 30°S-30°N, and 20°N-80°N, enhancing the sensitivity of the reconstruction to extra tropical variability, which is generally smaller than tropical variability. After the REOFs are computed for each region, they are merged with smoothing across the overlap regions.

For each region, a set of EOFs is computed using the GPCP.v2.1 monthly anomalies, 1979-2008. A maximum number of EOFs for each region is assigned and used for the reconstruction. The reconstruction finds weights for each of the EOFs for each month. The weights are determined by fitting the available gauge data to the set of EOFs. The weights minimize the mean-squared error between the reconstructed anomalies and the gauge data.

The maximum number of EOFs to use for each region is determined by cross-validation testing. In addition, each EOF from that maximum set must pass a screening test using the gauge sampling for each month or it will be excluded for that month's analysis. Cross-validation testing is also used to determine the screening level to use for the REOF in each region. The screening parameter for each EOF mode is the fraction of EOF variance sampled by the available sampling. Since the EOF variance at each point is proportional to the mode value squared, the fraction may be computed as the ratio of the squared EOF values summed over areas with sampling to the values summed over all areas.

Cross-validation testing is done by producing a set of EOFs for each region excluding the data for one year. This is done for every year, yielding 30 sets of EOFs for each region. In addition, data masks are developed to eliminate data where it was not available in several historical periods, here chosen to be the 30-year periods 1900-1929, 1930-1959, and 1960-1989. The GPCP.v2.1 data for the year as excluded from the EOF analysis is used to reconstruct that year, using each of the historical sampling grids. This simulates an analysis using historical sampling and EOF modes that are for the most part independent of the analysis year. Repeating this for every year gives the cross-validation reconstruction data, which are compared with the full data to evaluate the analysis. The global mean-squared error is used to determine the optimal values of the maximum number of modes and the screening parameter.

First the optimal maximum number of EOF modes is found using several screening parameters. After a stable maximum number of modes are found, the screening parameter is set using that maximum number. In Smith *et al.* (2008b) the

maximum number of modes was found to be 6 for the southern extra tropics, 12 for the tropics, and 11 for the northern extra tropics. Here the values for these three regions were found to be 5, 15, and 10, respectively. Thus, there was little change in the tuning of the maximum number of modes in each region. For all of these regions there was little change in mean-squared error when the screening parameter was set between 0.05 and 0.15, compared to changes outside that range. In Smith *et al.* (2008b) the sampling fraction was set to 0.05. However, here we find that some regions and historical grids were improved with slightly a higher screening parameter, and therefore we use 0.15 in the REOFs. This slightly higher value requires slightly more sampling for each mode compared to the earlier REOF. We hold these parameters constant and produce REOFs based on each of the three gauge analyses, discussed below.

In Smith *et al.* (2008b) a REOF was evaluated by regressing it against climate modes. The resulting regression maps were used to show the spatial reconstruction patterns associated with each mode. Here that is repeated for two important modes, the Southern Oscillation Index (SOI) and the North Atlantic Oscillation (NAO), using the same SOI and NAO index values. For the SOI regressions of all three REOFs yield similar patterns (Fig. 2), showing that the main ENSO mode is reflected in all reconstructions. Here and in the following discussions we refer to the GHCN-based REOF as REOF(GHCN), to the GPCC-based REOF as REOF(GPCC), and to the CRU-based REOF as REOF(CRU). The similarity of the spatial patterns indicates that for each the same reconstruction modes are used, with more or less the same relative importance. The difference in strength suggests that the REOF(CRU) is able to weight the set of modes used with more confidence due to its higher sampling over most of this period (Fig. 1).

A similar set of regressions is computed for the December-March average NAO (Fig. 3). As expected, the strongest and most consistent NAO regressions are in the North Atlantic. Strong and consistent patterns extend into Europe, North America, the Pacific, East Asia, and even the tropical Indian Ocean and parts of tropical Africa. NAO regression patterns also appear in the tropical Pacific in each, but they are less consistent than the patterns in the northern extra tropics. Overall, the NAO patterns from each regression are similar in both spatial pattern and strength.

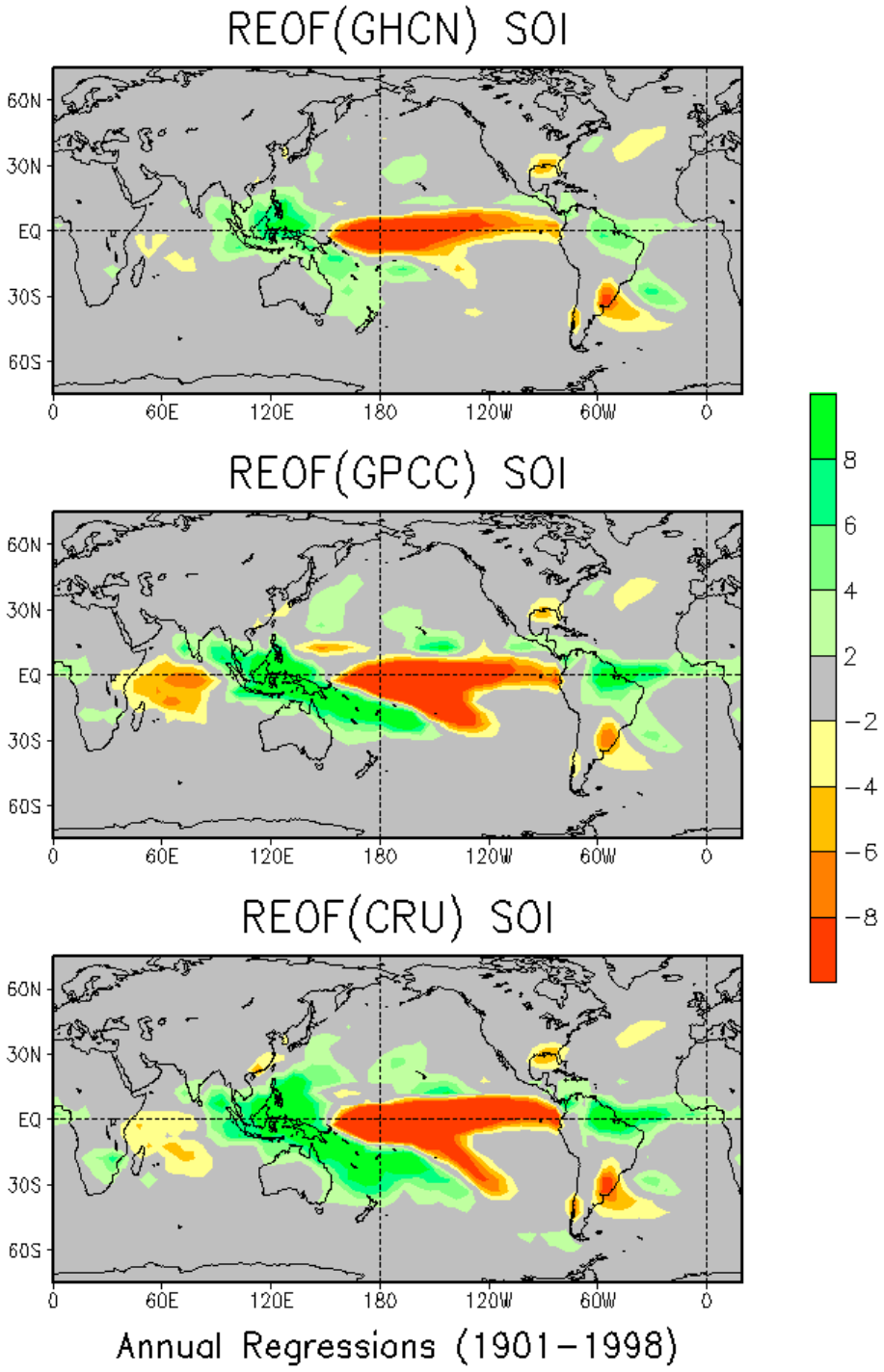

Figure 2. Regressions of each REOF against the SOI. REOFs are based on GHCN (upper), GPCC (middle) and CRU (lower panel). Annual averages of the index and REOFs are used over 1901-1998, when all are available. The SOI is normalized so the precipitation units are mm/mon per standard deviation.

The global spatial standard deviation for each historical REOF (Fig. 4) indicates the relative consistency of each over time. Here the monthly global spatial variance is computed, and then averaged annually before taking the square root to define the spatial standard deviation of each. REOF(GHCN) has lower values before 1950, when its sampling tends to be especially low (Fig. 1). After about 1990 the GHCN sampling also decreases, and there is a corresponding decrease in its REOF standard deviation in that period. Both the REOF(GPCC) and REOF(CRU) have more consistent values over most of the period. REOF(GPCC) has lower standard deviations before 1910, when it has less sampling. REOF(GPCC) has less of a drop off in sampling in the most recent years, and it maintains stronger standard deviation in those years, but it also has a high spike in 1997-1998 which is much larger than the others.

The GPCC gauge data are used in the GPCP satellite-gauge analysis, which is used to compute reconstruction statistics. This gives the GPCC an advantage in fitting to modes that include GPCC base data, and it helps to explain the higher standard deviation of the GPCP-based REOF, referred to as REOF(GPCP). However, errors in the satellite-period GPCC may be incorporated in the REOF statistics, and they may be partly reproduced in the REOF(GPCC). The other gauge analyses are not directly used in GPCP, so random errors in those analyses should be more different from any that influence the reconstruction statistics. Thus, there can be more filtering of errors by using a gauge analysis not used in the formation of the satellite-gauge analysis. The high REOF(GPCC) standard deviation in 1997-1998 is associated with a strong ENSO episode in that period, but its magnitude could be inflated by GPCC errors. To test this, the GPCP satellite-gauge data are filtered by computing a reconstruction using them. This is simply EOF filtering of the base data to eliminate variations not in the analysis modes. The variance of this filtered GPCP data is also shown on Fig. 4. The filtered GPCP data also contains a spike in 1997-1998, but it is not as strong as the one from the GPCC-based REOF, indicating that the REOF(GPCC) magnitude may be inflated. Overall, the REOF(CRU) has most consistent values over most of its record and for the overlap period before 1990 it yields values similar to the filtered GPCP.

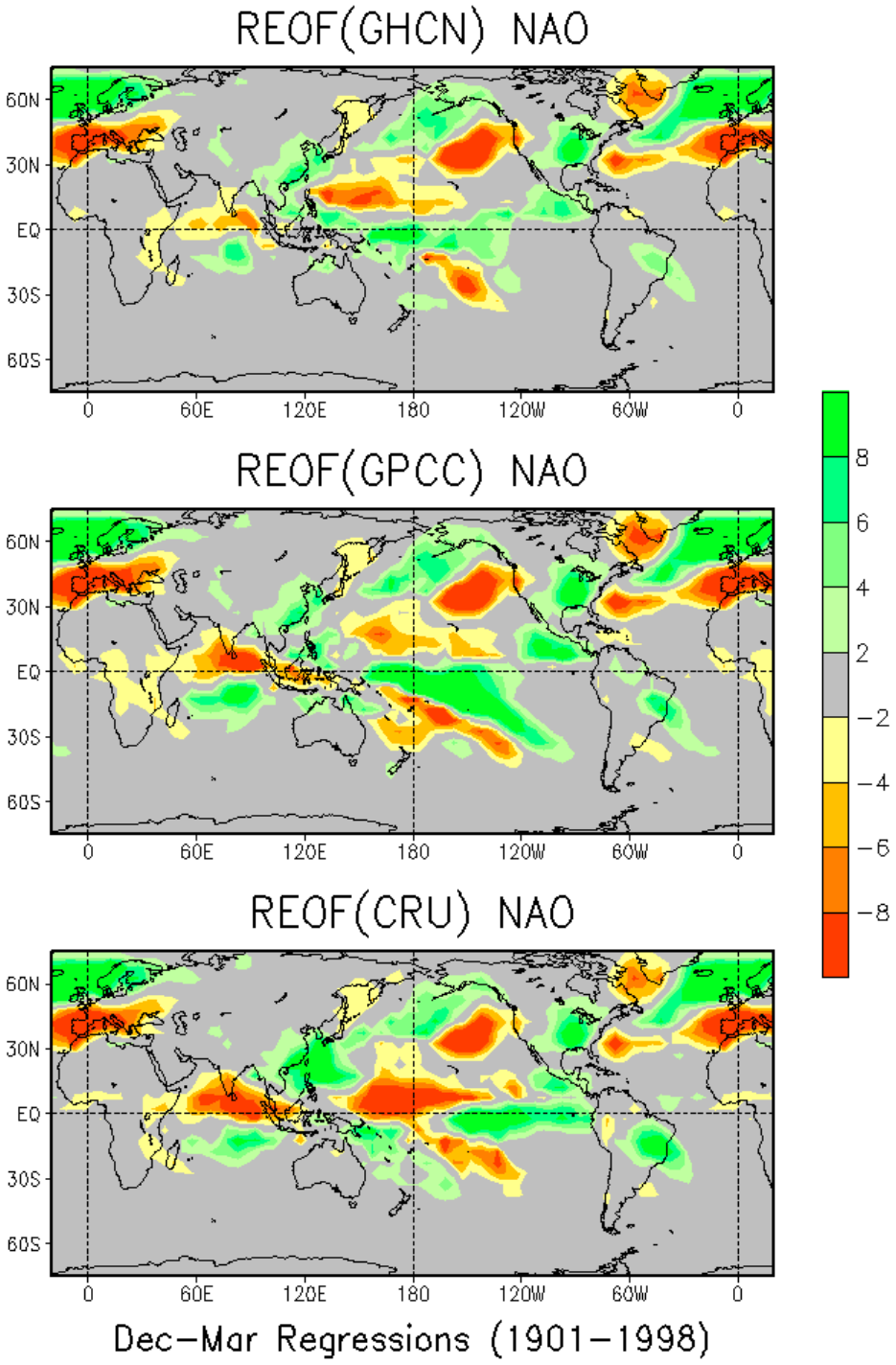

Figure 3. Regressions of each REOF against the NAO. REOFs are based on GHCN (upper), GPCC (middle) and CRU (lower panel). December to March averages of the index and REOFs are used over 1901-1998, when all are available. The NAO is normalized so the precipitation units are mm/mon per standard deviation.

For their common analysis period (1901-1998) global spatial correlations between pairs of REOFs are computed to better indicate when they are most similar (Fig. 5). Correlations against the REOF(GHCN) tend to be lowest early in the reconstruction period, when GHCN sampling is lowest. REOF(GPCC) and REOF(CRU) have roughly consistent correlations for their entire overlap period, and after 1950 the REOF(GHCN) and REOF(GPCC) correlations have similar values. Strongest correlations are between REOF(GHCN) and REOF(CRU) in 1950-1990. This strong correlation indicates that the two gauge analyses yield similar variations when sampling is sufficient in both.

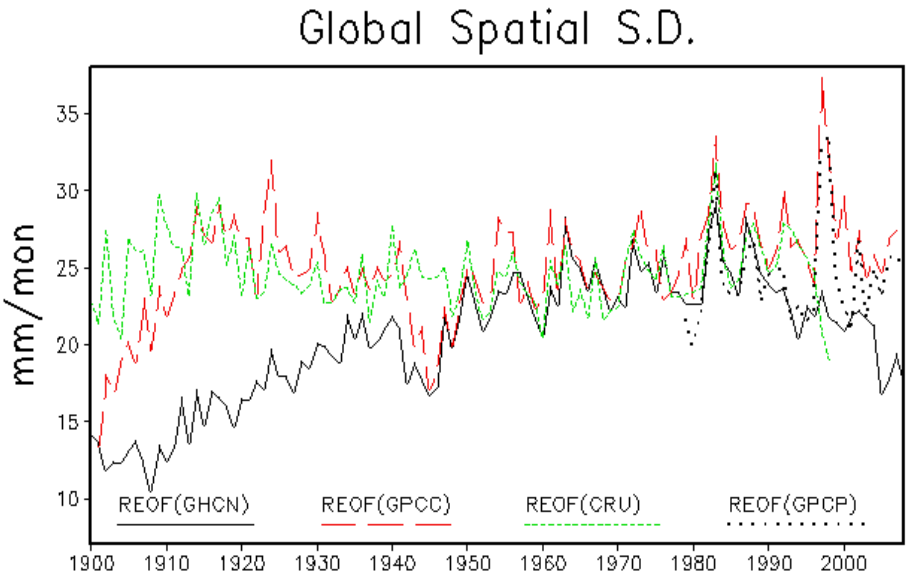

Figure 4. Global spatial standard deviation for each of the three REOFs and for the GPCP data filtered using the REOF modes. For plotting clarity the monthly spatial variance averaged to annual values and the square root of that is taken for the standard deviation.

These inter-comparisons between the three REOFs indicate that since about 1950 REOF(CRU) and REOF(GHCN) are similar, but early in the 20th century REOF(CRU) should be more reliable due to its better spatial sampling. The spatial standard deviations and correlations both indicate that the GHCN sampling is filtering out variations in the early 20th century due to sparse sampling. The GPCC has better sampling than either of the others in recent years, but it may artificially inflate variations as discussed above. Even in 1950-1990 when sampling is best for all gauge analyses, REOF(GPCC) typically has higher standard deviations than either of the other two, indicating that the GPCC may require more screening before it is used for a REOF.

Because REOF(CRU) has the most consistent variance over its entire reconstruction period, and also because of its consistency with REOF(GHCN) since 1950, we use REOF(CRU) for 1900-1978. Since the CRU gauge analysis is not updated through the entire period and sampling becomes sparse near the end of the 20th century a different REOF is required for the end of the period. Therefore, after 1988 we will use REOF(GPCP). From 1979 to 1988 we smoothly merge the two, using linear weights so that in 1978 the blended REOF is all REOF(CRU) and in 1989 it is all REOF(GPCP).

Since the two have similar variance in the overlap period, this blending should not cause a shift in the overall variance of the analysis. We refer to this blended analysis as the REOF(Blend) analysis. This common overlap period, 1979-1988, is also used as a re-centering period. The averages of anomalies are all forced to equal zero over this period in the comparisons that follow.

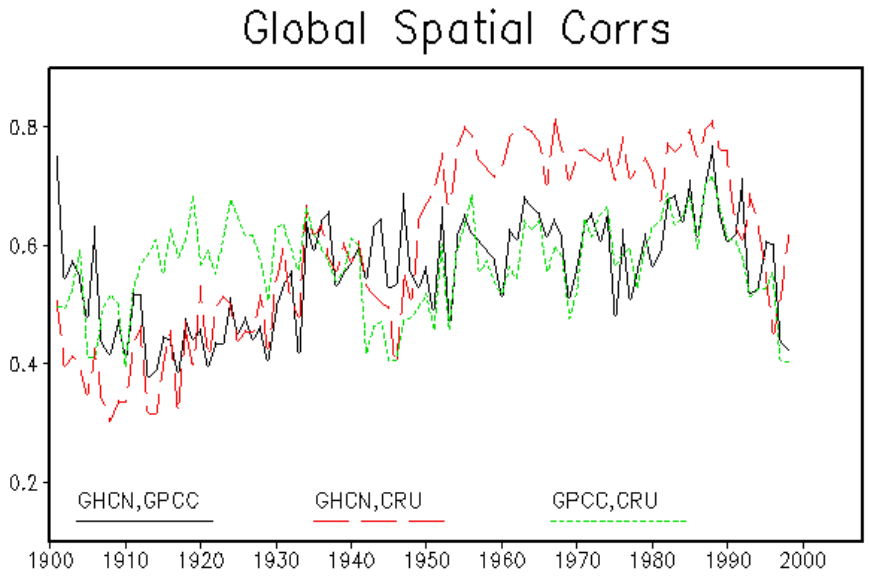

Figure 5. Global spatial correlations between pairs of REOFs. Each REOF is based on a gauge analysis, and the pairs correlated are indicated on the figure. For plotting clarity monthly correlations are averaged to annual values.

In Smith *et al.* (2008b), it was shown that the REOF method realistically reconstructs interannual variations, but it may be less reliable for representing multi-decadal variations. Here the reconstructions are compared for global averages over both land and ocean, separately. The annual and global averages are first computed, and then filtered using a seven-year low-pass filter to more clearly show the multi-decadal variations. The low-pass weights for the annual average are (0.032, 0.110, 0.220, 0.276, 0.220, 0.110, 0.032), which are close to binomial weights for a nine year filter with the end years eliminated.

The land-average multi-decadal variations are similar for all three (Fig. 6). REOF(GHCN) is more damped than the others before 1950, but all are similar afterwards. REOF(GPCP) is similar to the others for most of the overlap period, but it shows a sharp increase in the last several years when REOF(GHCN) is damped due to a drop off in sampling. The recent increase is partly reflected in REOF(GPCC), which ends a year before REOF(GPCP).

Over oceans (Fig. 7), there are greater differences in the first half of the 20th century. Part of the difference is due to damping of anomalies towards zero when data are sparse and fewer modes may be selected for use in the REOF. Differences may also be due to the fact that most ocean locations are remote from gauge sampling. The

oceanic component of the historical REOFs depends on large-scale teleconnections from the leading modes. Over land this is less critical because there are many local data to adjust the analysis. Without similar local oceanic data, the oceanic REOF multi-decadal variations may be less reliable than similar variations over land.

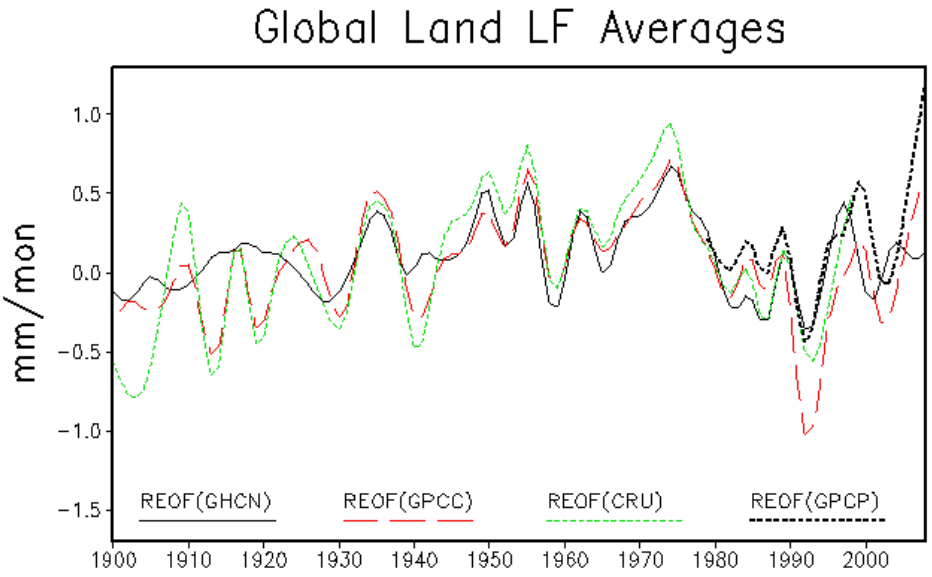

Figure 6. Low-pass filtered annual-global averages over land areas for each of the indicated REOFs. The REOF(GPCP) is the GPCP data filtered using the reconstruction modes.

Differences in the oceanic multi-decadal signals from earlier REOF analyses were discussed by Smith *et al.* (2008b), and they inspired Smith *et al.* (2009) to develop an indirect reconstruction method for resolving oceanic multi-decadal variations. That method reconstructs precipitation anomalies using locally observed oceanic variables related to precipitation in addition to teleconnections. That indirect method, described in the following subsection, was found to yield results more consistent with theoretical estimates of multi-decadal precipitation estimates.

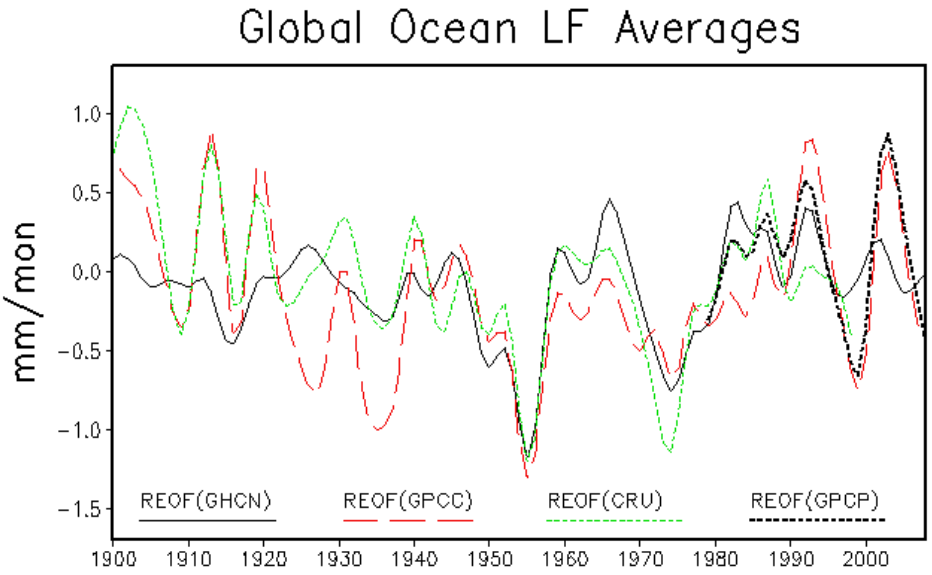

Figure 7. Low-pass filtered annual-global averages over ocean areas for each of the indicated REOFs. The REOF(GPCP) is the GPCP data filtered using the reconstruction modes.

2.3 RCCA

The reconstruction using canonical correlation analysis (RCCA) was discussed in detail by Smith *et al.* (2009). Canonical correlation analysis (CCA) was used by Barnett and Preisendorfer (1987) to forecast North American temperatures using SST and SLP predictors. The CCA finds correlations between fields of predictors and a predictand field, which can then be used to estimate the predictand field at some other time when only the predictors are available. Historical monthly reconstructions of SST and SLP are available for the 20th century, based mostly on ship observations of these variables. On long time scales, there tend to be relationships between the SST and SLP anomalies and precipitation anomalies. This allows us to use data from the GPCP period to define those relationships, and then use those relationships to reconstruct precipitation anomalies at times before the satellite period. Smith *et al.* (2009) found that most relationships reflected in the RCCA have time scales of seasonal or longer, and they therefore produced their RCCA for annual average anomalies. Here we do the same, except that we use the updated GPCP.v2.1 data.

The CCA decomposes predictor and predictand fields into spatial modes, and computes a set of CCA predictor-predictand modes that along with weighting factors are used for the analysis. One weighting factor defines the relative variance accounted for by each CCA mode, and the other is computed from the predictor data. The CCA used here has a cut off, so that it does not use any CCA modes that account for less than 1% of the variance of the first CCA mode. The RCCA training period is 1979-2004, from the first year of the satellite period to the last year of the SLP analysis. Updates to the SLP data are available for years beyond 2004, but those updates are computed differently and they have larger spatial variations than the historical SLP data. We therefore do not use them

for training the model to keep those differences from producing spurious variations in the correlation relationships. However, we do use the SLP updates to extend the reconstruction through 2008. The greater SLP spatial variations should be largely filtered out by the CCA modes computed using data without them.

The RCCA predictor fields are filled for all historical years, so it is not necessary to tune the number of RCCA modes for different sampling conditions. However, the number of RCCA modes should be tuned to ensure that the optimal amount of variance is reconstructed. Here cross-validation tests are performed that compute the RCCA for each year using training data that excludes the analysis year. For each of the cross-validation years the RCCA used nine or ten modes, although nine were used more often than ten and the tenth mode never added more than a small fraction of the variance. Usually the tenth and higher modes were truncated since they accounted for less than 1% of the first mode's variance. Thus, we perform our RCCA using nine modes. However, testing using fewer modes showed that most multi-decadal variations were retained using as few as three modes.

2.4 Comparing REOF and RCCA

Next we compare the REOF and RCCA estimates over both land and ocean areas. The REOF discussed here is the blend of REOF(CRU) and REOF(GPCP) described above, and referred to as REOF(Blend). As with the comparisons above, global land and ocean-area averages are used in these comparisons.

Over land the different estimates are all correlated in their interannual variations. The larger variations in the CRU gauge data are more closely matched by the REOF(Blend) when it is sub-sampled at gauge locations (shown by the thin dotted black line). Both the REOF(Blend) and the CRU gauges indicate a positive trend over the period, but the RCCA indicates a negative trend over the period (see Table 1). Because local gauge data anchor the land area REOF(Blend), it should be better able to better represent variations over land compared to its oceanic variations. By comparison, the RCCA land analysis does not use gauges, and depends heavily on teleconnections from ocean areas driven by the SSTs. The SLP anomalies over land are used, but they are still indirect indicators of precipitation. In regions near to where data are available, direct reconstructions using those data should be superior to indirect reconstructions. Therefore, the REOF(Blend) should be used over land regions.

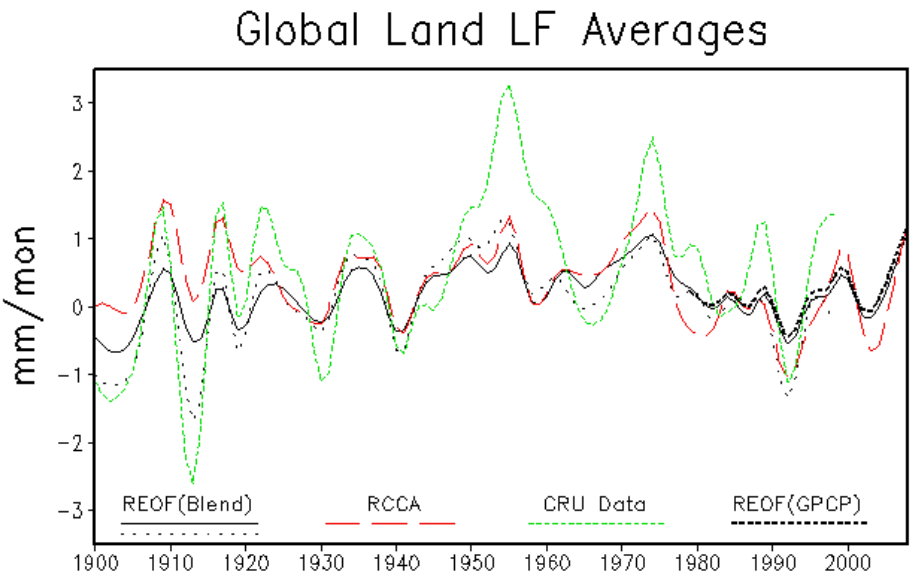

Figure 8. Low-pass filtered annual-global averages over land areas for each of the indicated estimates. For the REOF(Blend), the solid line is averages over all land area and the dotted line is averages only over areas with CRU gauge sampling.

Averages over ocean areas are similar for the REOF(Blend) and RCCA for most of the satellite period. But before 1980 they diverge, with the REOF(Blend) indicating a negative trend and the RCCA indicating a positive trend. In addition, the REOF(Blend) does not resolve the 1970s climate shift, which is associated with a rapid change in Pacific SSTs (Trenberth and Hurrell 1994, Zhang *et al.* 1997). The RCCA increasing precipitation and 1970s climate shift are modeled from correlations with the Pacific SST variations. The ocean-area average AR4 indicates a weaker but consistent positive trend, which is the theoretical response to a warming Earth (Held and Soden 2006, Allan and Soden 2008). There is also some observational evidence from satellites for overall increasing precipitation (Adler *et al.* 2008). The ability of the RCCA to resolve these oceanic variations, consistent with known and theoretical climate variations, suggests that its multi-decadal signal is superior to the REOF(Blend) multi-decadal signal over oceans. The local SST data over oceans allows the RCCA to better resolve these variations.

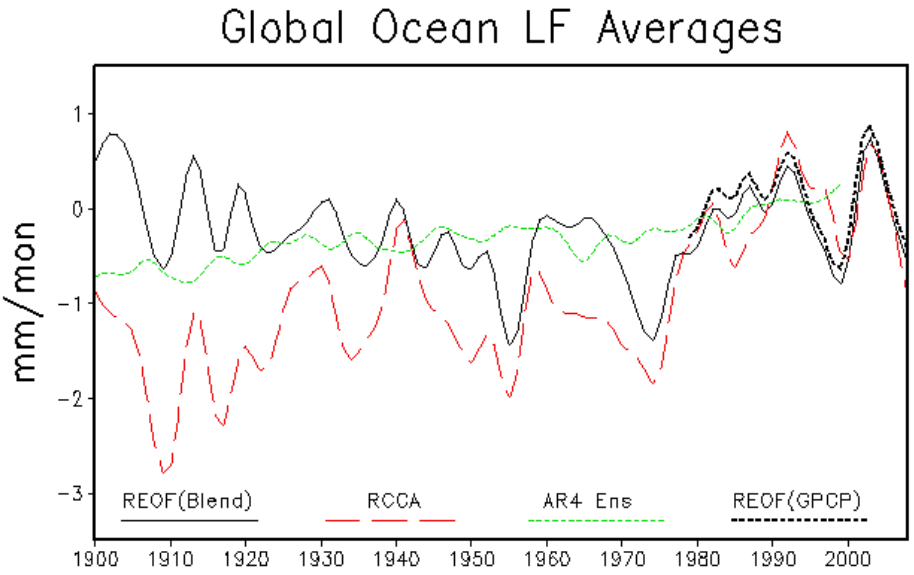

Figure 9. Low-pass filtered annual-global averages over ocean areas for each of the indicated estimates.

Although the multi-decadal variations are not linear trends, examination of trends is useful for evaluating overall changes of different estimates. Table 1 shows trends from several reconstructions, the AR4 model ensemble, and gauges. Note that the RCCA has a strong positive ocean-area trend, but its land-area trend is negative. The RCCA difference in sign between ocean and land trends may be due to the generally opposite tendency in precipitation anomalies associated with ENSO episodes (Adler et al. 2008). The RCCA ENSO modes are developed from interannual variations, and are used for modeling variations on longer time scales that can include ENSO-like variations (Zhang *et al.* 1997). Because the GPCP record is only 30 years long, its modes may not span all multi-decadal variations. If the ENSO-like low-frequency variations have opposite land-sea precipitation tendencies, similar to interannual ENSO variations, then the opposite tendency in the RCCA may be correct. A similar ocean-land difference is evident for the AR4 ensemble trends, except that the AR4 trends are weaker. It is possible that the AR4 models are mimicking the interannual ENSO-mode tendency for opposite precipitation anomalies over land and sea.

The CRU gauge data and the land REOF(Blend) both suggest that this tendency for opposite precipitation anomalies over land and sea may not hold up on multi-decadal time scales. Both of those estimates show positive trends over land areas. This shows the importance of local data, either direct observations of precipitation or indirect indicators of it, for producing reconstructions using imperfect teleconnection patterns. Local data can force reconstructions to better reflect local variations. When only remote data are available the reconstruction is at the mercy of the teleconnections resolved by the available modes.

In the following section we show how to merge the REOF(Blend) and RCCA retaining the best features of each. Because we do not have independent validation for

oceanic regions, we must infer what oceanic features are most realistic based on the physical arguments outlined above. An almost complete lack of direct observations of oceanic precipitation before the satellite era also makes it difficult to estimate the full analysis uncertainty. Therefore, this analysis is best used qualitatively over oceanic regions. However, its tuning against GPCP makes its values realistic, within the limits of GPCP to estimate realistic oceanic values.

Table 1. Trends of low-pass filtered annual-global averages of the indicated estimate, averaged over land areas, ocean areas, and all areas. The REOF analysis is the blended REOF(CRU) and REOF(GPCP), and REOF(G) indicates using only sampling at CRU gauge locations. All trends are over 1900-1998, and units are mm/mon/100 years.

Estimate	Land	Ocean	All Areas
RCCA	-0.5	1.6	0.7
AR4	-0.1	0.7	0.4
REOF	0.4	-0.4	-0.1
REOF(G)	0.4	----	----
CRU Gauges	1.2	----	----

3. Merging REOF(Blend) and RCCA

This section describes merging two reconstructions, REOF(Blend) and RCCA. The blended REOF uses REOF(CRU) through 1978, REOF(GPCP) after 1988, and a smooth blend of the two in-between. This additional step merges that blended REOF with the RCCA by bias adjusting the REOF(Blend) using the RCCA multi-decadal signal.

As discussed above, the multi-decadal component of an analysis can be approximated by filtering annual averages to remove most interannual variations. In the sections above and here we filtered over seven years using the following annual weights: 0.032, 0.110, 0.220, 0.276, 0.220, 0.110, 0.032. These are approximately the binomial weights for a nine-year filter with the end years removed. The figures in Section 2 illustrate the effect of this filter.

This filter was chosen after performing a number of tests on an earlier REOF analysis using GPCP base data and GHCN gauge data. First a set of running-mean filters were tested with lengths from five to 21 years. They showed that filter lengths of between five and eleven years removes almost all of the interannual variations. Based on these results a five to seven-year filter should be adequate for filtering. In order to minimize aliasing we used the near-binomial seven-year filter. The weights for this give most weight to the middle five years of the average. Applying this filter to the GPCP monthly anomalies and subtracting the resulting multi-decadal signal from the GPCP anomalies left more than 90% of the variance in the residual. Thus, we can expect that

removing the signal defined by this seven-year filter will leave nearly all the interannual variations in the REOF analysis.

In Section 2 we show that over the oceans the REOF(Blend) multi-decadal signal is suspect for most of its record length when there are only sparse island and coastal gauges to anchor the analysis. Oceanic regions are bias adjusted so that their multi-decadal variations match the RCCA multi-decadal variations. To achieve this, the REOF(Blend) is annually averaged and filtered using the seven annual weights. This defines the raw REOF(Blend) multi-decadal signal. The annual RCCA analysis is similarly filtered to define its multi-decadal signal. Both annual multi-decadal signals are interpolated from annual to monthly averages. The ocean-area monthly-interpolated REOF(Blend) multi-decadal signal is then subtracted from the REOF(Blend) analysis and the monthly-interpolated RCCA multi-decadal signal is added onto it.

Land regions do not require bias adjustment since they are well sampled by the gauges, which are assumed here to be unbiased. Since land regions are not adjusted, the adjustment weight for 5° regions that are all land is zero. The adjustment weight for regions that are all ocean is one, and for coastal and island regions the weight is between 0 and 1, depending on the fraction of land area. Because the land REOF(Blend) multi-decadal signal is similar to the RCCA multi-decadal signal, coastal discontinuities in the multi-decadal signal are minimal. The REOF(Blend) uses the REOF(GPCP) data after 1988, which gives it good oceanic sampling for the recent period. Thus, it should not be necessary to bias adjust it for the most recent years and for any updates to the analysis that we may wish to produce. Therefore, the bias adjustment is allowed to decay linearly from full strength in 1989 to zero in 1999. Because the REOF(GPCP) heavily filters the GPCP, we should be able to use future updated versions of GPCP to update the analysis without introducing inhomogeneities.

We also tested an analysis in which the RCCA anomalies are statistically re-injected into the bias adjusted REOF(Blend). This could possibly improve skill if the annual RCCA contains variations that are not well represented in the annual bias adjusted REOF(Blend). The RCCA re-injection used an optimal interpolation method to assign weights for the RCCA and bias adjusted REOF(Blend), with weights inversely proportional to their errors measured against GPCP. The weights were forced to sum to 1 so that there would be no damping of anomalies. We found that the analysis with re-injected RCCA had lower variance than the bias adjusted REOF(Blend) almost everywhere, including in the Southern Ocean where the REOFs use the fewest reconstruction modes. Since that variance damping is undesirable we do not use the analysis with re-injected RCCA.

4. Error Estimates

Error estimates are computed for the merged analysis, for maps and for averaged data. We divide the error estimate into two parts, a sampling error and a bias error. The sampling error variance is computed by finding the fraction of the variance resolved by the analysis and subtracting that from the total variance. Here we use the REOF(GPCP) variance as the total variance, since that filtered data represent the climate-scale precipitation variations that this analysis attempts to resolve using historical data. When monthly errors are computed, variance is computed separately for each month.

The mean-squared error of the reconstruction is defined as

$$E^2 = \left\langle (R - P)^2 \right\rangle . \qquad (1)$$

Here *R* is the reconstruction and *P* is the true precipitation anomaly, and the brackets denote averaging. By expanding equation (1) we can obtain

$$E^2 = \sigma_R^2 + \sigma^2 - 2\sigma_R \sigma r + (\langle R \rangle - \langle P \rangle)^2 . \qquad (2)$$

Here σ_R^2 is the reconstruction variance, σ^2 is the true precipitation variance, and r is the correlation between the reconstruction and the true precipitation. The first three terms on the right-hand side of equation (2) account for the sampling and random error variance, $E_S^2 = \sigma_R^2 + \sigma^2 - 2\sigma_R \sigma r$. The last term on the right-hand side of equation (2) accounts for the mean bias error variance, $E_B^2 = (\langle R \rangle - \langle P \rangle)^2$. We will consider these error components separately in their estimation.

The random error, due to noise in the analysis, should be a small fraction of the total error. That is because the reconstructions are produced by filtering data using spatial modes, which will filter out most noise. Thus, we will assume that the final reconstruction noise is negligible and deal with the sampling error component.

The correlation squared, r^2, defines the fraction of the variance accounted for by the reconstruction. By ignoring random noise we can estimate this from $r^2 \approx \frac{\sigma_R^2}{\sigma^2}$. This makes it possible to estimate the sampling error variance as

$$E_S^2 = \sigma_R^2 + \sigma^2 - 2\sigma_R \sigma r \approx \sigma^2 - \sigma_R^2 . \qquad (3)$$

The reconstruction anomaly variance can be estimated directly from the analysis and the true precipitation anomaly variance can be estimated from the base-period data. The sampling error variance is simply the variance not accounted for by the reconstruction.

For the sampling error variance, we are here most interested in how well the climate-scale features of precipitation anomalies are resolved. Thus, for our estimate of the true variance we do not use the full GPCP.v2.1 variance, but rather we use the variance of the REOF(GPCP). The filtering removes small-scale variations, but because of satellite sampling in the data it retains sampling of all climate-scale variations. This choice is made in order to evaluate the sampling error relative to the best that could be done with complete sampling for this analysis method. It is not an absolute measure of error, but it is a measure of relative error from one time to another. Comparisons of our results in the satellite period can help users to calibrate our error estimates against the full data, to help guide users of these data.

Over land the gauges that anchor the land REOF(Blend) are assumed to be unbiased, suggesting that the land bias error should be low. Figure 8 shows that the large-scale low-pass land REOF(Blend) is often close to the similarly filtered gauge data when common sampling is used for both. Before 1940 the differences in the two tend to be less, while after 1940 they are often much larger. Since these gauge data are used for the REOF(Blend), differences must be due to the REOF(Blend) modes filtering variations out of the gauge data. Differences should not be due to sparse sampling, since after 1940 there is good sampling of the gauge data (Fig. 1). Differences could be in part due to reconstruction using too few modes to fully resolve some land variations. The modes most important for some historical periods may be excluded from the limited set of modes most important for the base period, which are used for the REOF(Blend).

Here we simplify the land bias estimate by ignoring systematic differences that may be caused by systematic under representation by the available REOF modes. Thus, if all REOF modes are used then there will be no land REOF(Blend) bias error in this analysis, since the gauges are assumed to be unbiased. If fewer REOF modes are used then errors will be represented in the sampling error component discussed above. Making this assumption allows the errors to be estimated, although it may cause an under estimation of total error in some periods. Thus, we again can not claim to measure absolute error, but we can give an estimate of the relative error from one period to another.

Over oceans the multi-decadal signal of both reconstructions is forced to match the RCCA multi-decadal signal. The RCCA bias error variance is estimated using the bias errors likely to contaminate the SST and SLP forcing data in the RCCA. Bias errors for these forcing fields are discussed by Smith *et al.* (2008a) for SST and by Allan and Ansell (2006). Because these biases are only approximately known they are roughly estimated to evaluate their approximate influence on the RCCA bias estimates. Here the SST bias uncertainty standard error is set to its global value, which is about 0.06ºC or less before 1939 (Rayner *et al.* 2006). From 1939 to 1941 it is damped linearly each year down to 0.015ºC in 1941. It is held at that level for the remaining years of the analysis. The larger values earlier in the period are due to the need for a large historical bias adjustment in that period when different types of buckets were typically used to measure SSTs. In more recent years the sampling is more consistent and SSTs have smaller biases, but there are still different sampling methods and the smaller standard error

estimate is used to account for SST bias uncertainties in the most recent period. The SLP bias standard error has not been studied as extensively. Therefore, we here estimate it to be 0.25 times the SLP anomaly standard deviation, and hold it constant in time in order to compute bias error estimates. The actual bias uncertainty should be much less than the standard deviation, so this crude estimate may be larger than the actual value. In the resulting RCCA runs, the SST bias standard error dominates the resulting bias uncertainty estimates.

We perform three RCCAs to evaluate bias uncertainty. One is forced with SSTs equal to their bias standard error and SLPs set to zero, the second with SSTs set to zero and SLPs set to their bias standard error, and the third with both SSTs and SLPs set to their bias standard errors. The standard errors from all three are averaged to estimate the RCCA standard errors. If errors of spatial or temporal averages are desired then the standard errors from all three are also averaged. Typical values for 5º annual estimates are ±6 mm/mon. Averaging reduces the magnitude of the bias error since the modes force both positive and negative values. Averaging over all (land and ocean RCCA areas) reduces the bias errors for the global average to 0.05 mm/mon for 1900-1938, down to below 0.01 mm/mon for 1941 onward.

Using these methods errors can be computed for monthly maps or for spatial or temporal averages. For the sampling error all that is needed is to average or filter the data before computing the variances used in equation (3). For the bias error, the filtered monthly bias maps are similarly averaged or filtered before evaluating differences. Although useful as a first-order estimate of analysis uncertainty, these error estimates are still crude and in the future we may be able to refine our error estimates.

5. Merged Precipitation Anomalies

Here the blended bias adjusted reconstruction is discussed and compared with other analyses. First the overall variations are examined to see how they may change in time with changes in the data used for reconstructions. As discussed earlier, the analysis filtering using spatial modes should remove nearly all random noise, and the largest sampling errors are likely to be from under-representation of variations. An overall measure of analysis strength is provided by the spatial standard deviation. The global spatial variance is computed monthly, and then annually averaged for plotting clarity before the square root is taken. We show spatial standard deviation time series for the bias adjusted REOF(Blend), the RCCA, the REOF(GPCP) and GPCP (Fig. 10). For consistency, the RCCA values were interpolated to monthly values before computing spatial statistics.

The adjusted REOF(Blend) has systematically higher standard deviation than the RCCA, although both indicate ENSO variations over the analysis period. In addition, both adjusted REOF(Blend) and RCCA have little trend in their spatial standard deviations, suggesting that sparse sampling early in the 20th century is not causing the analyses to be damped in that period. For REOF(GPCP) standard deviation is consistent

with values for the adjusted REOF(Blend) in earlier periods. Both have similar averages with little apparent trend, and both have similar magnitudes of changes with ENSO episodes, although the 1997-98 episode is larger than others. This indicates that blending with the adjusted REOF(GPCP) should not cause variance jumps relative to the earlier period. The GPCP standard deviation is largest of all, because those data are not filtered with spatial modes and they represent all satellite and gauge spatial variations. In addition, the GPCP standard deviation has a trend from before 1990, when infrared-based satellite estimates dominate the analysis, to the later years when microwave-based satellite estimates are used. The microwave-based satellite estimates have higher spatial resolution, and this trend in the GPCP standard deviation reflects the change in instruments used rather than changes in precipitation. Filtering in REOF(GPCP) removes this trend.

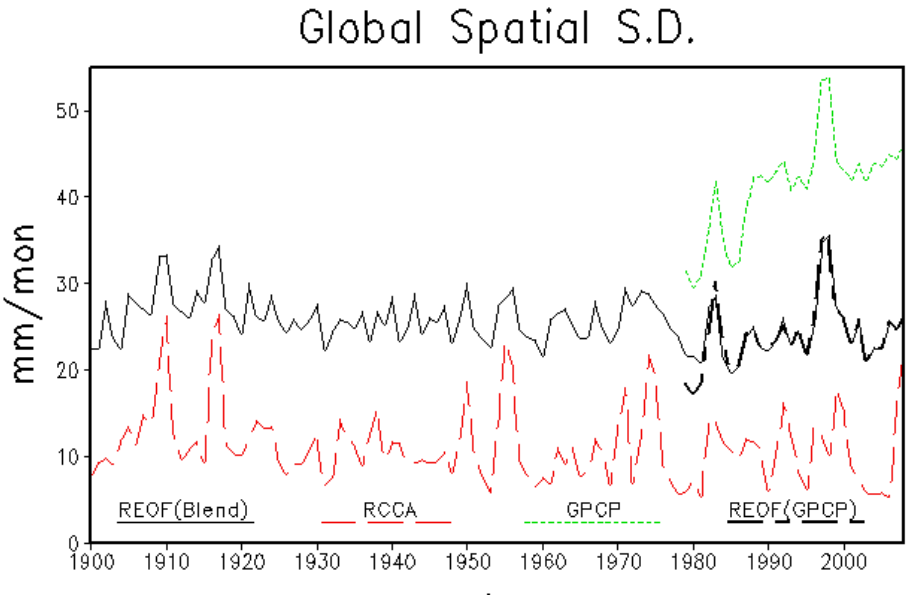

Figure 10. Global spatial standard deviations for the indicated analyses. The REOF(Blend) is bias adjusted over oceans using the multi-decadal RCCA. For plotting clarity the monthly spatial variance is averaged to annual values and the square root of that is taken for the standard deviation.

The bias adjusted REOF(Blend) with the seven-year low-pass filter applied is shown for averages over the global oceans (Fig. 11) and averages over all ocean and land areas (Fig. 12). Over the oceans, this is the same as the RCCA low-pass average. The uncertainty estimates are about 0.5 mm/mon early in the period, shrinking to less than half that by the end of the period. Much of this error is due to bias error from the RCCA, but the sampling error component also contributes to errors early in the analysis period. Near the end of the analysis period most of the error is from bias errors. Bias errors are largest before 1940 when the bias uncertainty is largest, due to the need for SST bias adjustments that can affect the RCCA.

Combined ocean and land averages (Fig. 12) have an increase over the 20th century similar to the ocean averages, but the increase is not as strong when land areas

are included. Note that the vertical scale for the all-area average has a smaller range than the scale for the ocean-area average and combining land and ocean areas reduces the multi-decadal changes. In addition, for the total area the 1970s climate shift is not apparent and there are fewer variations with time scales shorter than ten years. The error estimates are also smaller for the all-area average, with largest values between about 1940 and 1990 due to an increase in the sampling-error estimate over that period. After 1990 errors are smaller. Note that the sampling-error estimate used here is computed from the difference in variance between the base data and the historical reconstruction. It uses the assumption that the variance is roughly stationary, and it does not use any measure of the actual sampling. Thus it should be considered a crude estimate of the sampling error. The mid-century inflation in estimated global all area sampling error is likely influenced by changes in SST and SLP sampling, which affects the RCCA variance. But much of the variance is contributed by the climate modes such as ENSO and NAO, and periods with less activity in these modes compared to the base period will show higher sampling error as estimated by our methods.

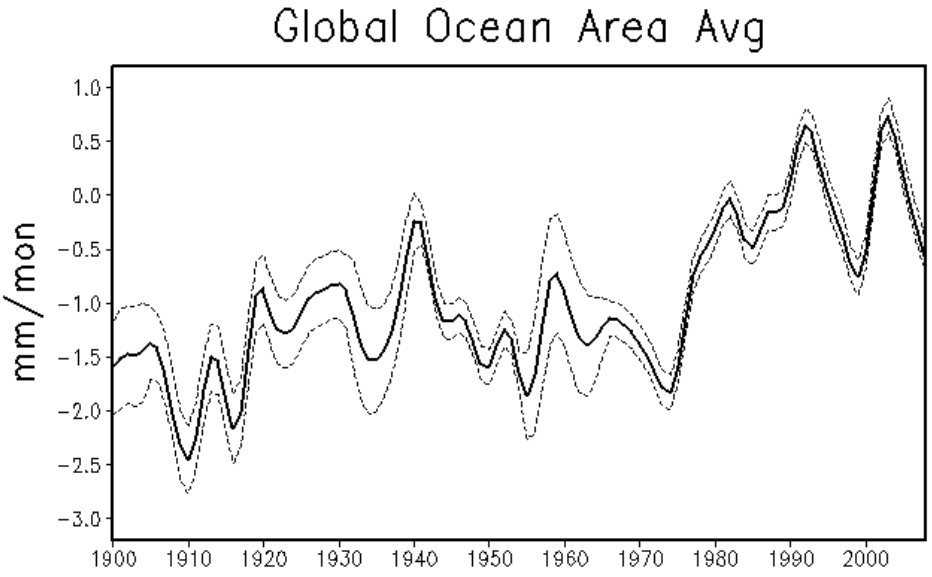

Figure 11. Global ocean area average bias adjusted REOF(Blend) with the 7-year low-pass filter applied, with 95% confidence interval estimates.

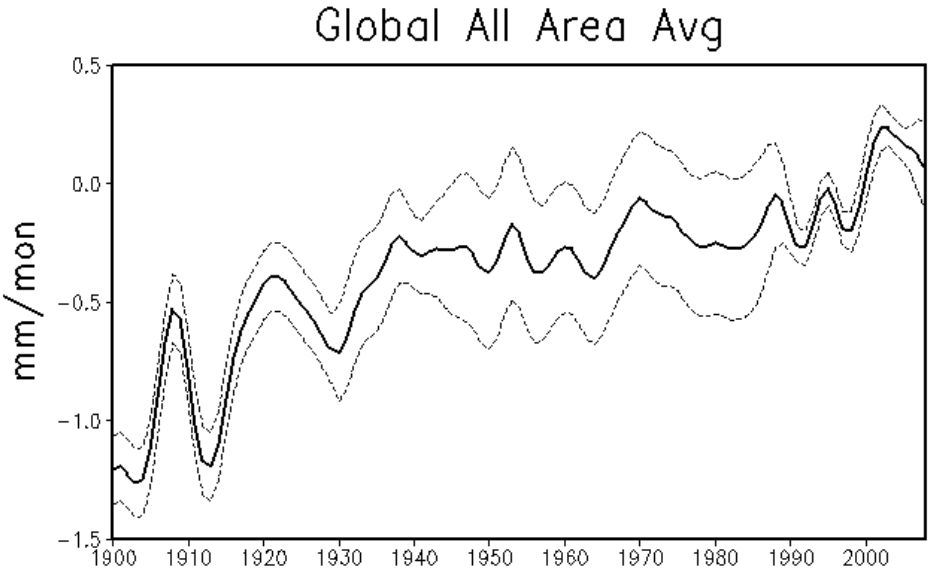

Figure 12. Global ocean and land area average bias adjusted REOF(Blend) with the 7-year low-pass filter applied, with 95% confidence interval estimates.

The tendency and strength of the analysis are next evaluated using the linear trend over the analysis period and the standard deviation (Fig. 13). For both monthly anomalies are used. The trend is scaled so that it may be plotted using the same shading as the standard deviation. The trends are clearly strongest over the oceans, where the RCCA multi-decadal component defines them. However, there are variations over land, including a positive trend over the eastern U.S. There is also consistency between oceanic and land trends in several places, including south-east South America, north-east South America, the west coast of North America, and northern Australia.

The standard deviation shows that strongest variations are over the tropics, but there are secondary maxima over the northern mid latitudes associated with extra-tropical storm tracks. There is much less variation in the Southern Ocean, where the REOF analysis has only five modes due to the lack of gauge sampling in that region.

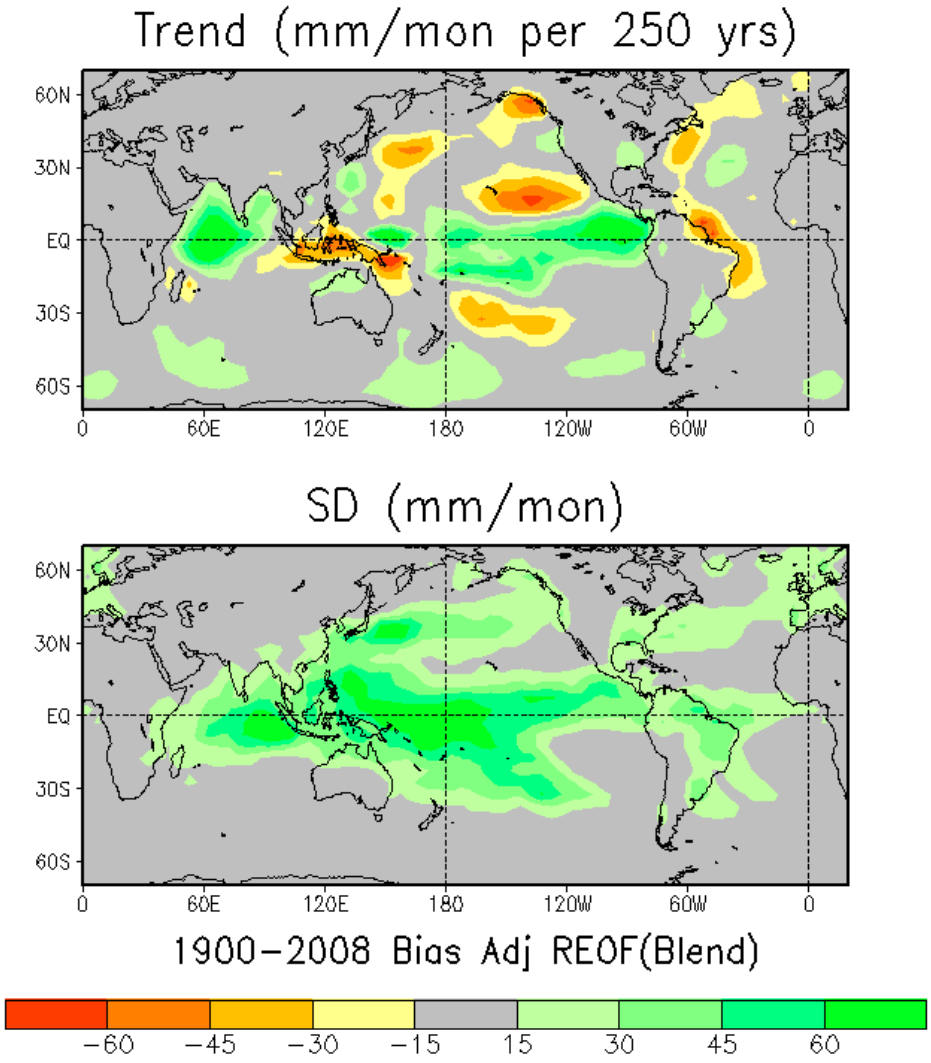

Figure 13. Linear trend (upper panel) and standard deviation (lower panel) of bias adjusted REOF(Blend) monthly anomalies, 1900-2008.

Much of the variation in the Southern Ocean comes from the RCCA component of the analysis, as indicated by the standard deviation ratio of low-pass filtered data to the unfiltered standard deviation (Fig. 14, upper panel). The low-pass standard deviation is also large fraction of the whole in the south-east Pacific and Atlantic, which are normally dry, and in the Arabian Sea and off the west coast of North America and North Africa. Over regions dominated by extra-tropical cyclones the low-pass standard deviation is a small fraction of the total standard deviation. The fraction of the trend standard deviation to the low-pass data standard deviation is high in many of the same places where the low-pass data accounts for much of the variation (Fig. 14, lower panel). This indicates that where the low-pass standard deviation is relatively strong, much of its variation is explained by a linear trend. Trends account for much of the variation over the Southern Ocean, where the trend itself is positive and relatively weak (Fig. 13, upper panel). A positive trend is also important over the eastern tropical Pacific, which influences ENSO-

like variations. Off the south-west coast of North America a negative trend is important, in the mid-latitude subsidence zone. The trends are strongest over the oceans but they can influence adjacent land regions.

The differences in overall land and ocean trends are a bit clearer when zonal averages of each are compared (Fig. 15). The ocean-area trends are stronger, especially in the tropics. Over the oceans there is a positive trend in the tropics and a negative trend en each hemisphere in the sub-tropics. In the Northern Hemisphere there is a negative ocean trend in the extra tropics while in the Southern Hemisphere the ocean trend becomes positive south of about 40ºS. The land-area trends are weaker and generally negatively correlated with the ocean-area trends. In the tropics the land trend is negative, with more positive trends in the sub-tropics at latitudes where the ocean trends are negative. Just south of 30ºN there is a weak negative land trend, with a weak positive land trend just north of 30ºN. This is consistent with slight drying in the Northern Hemisphere desert zones and increasing precipitation in eastern North America.

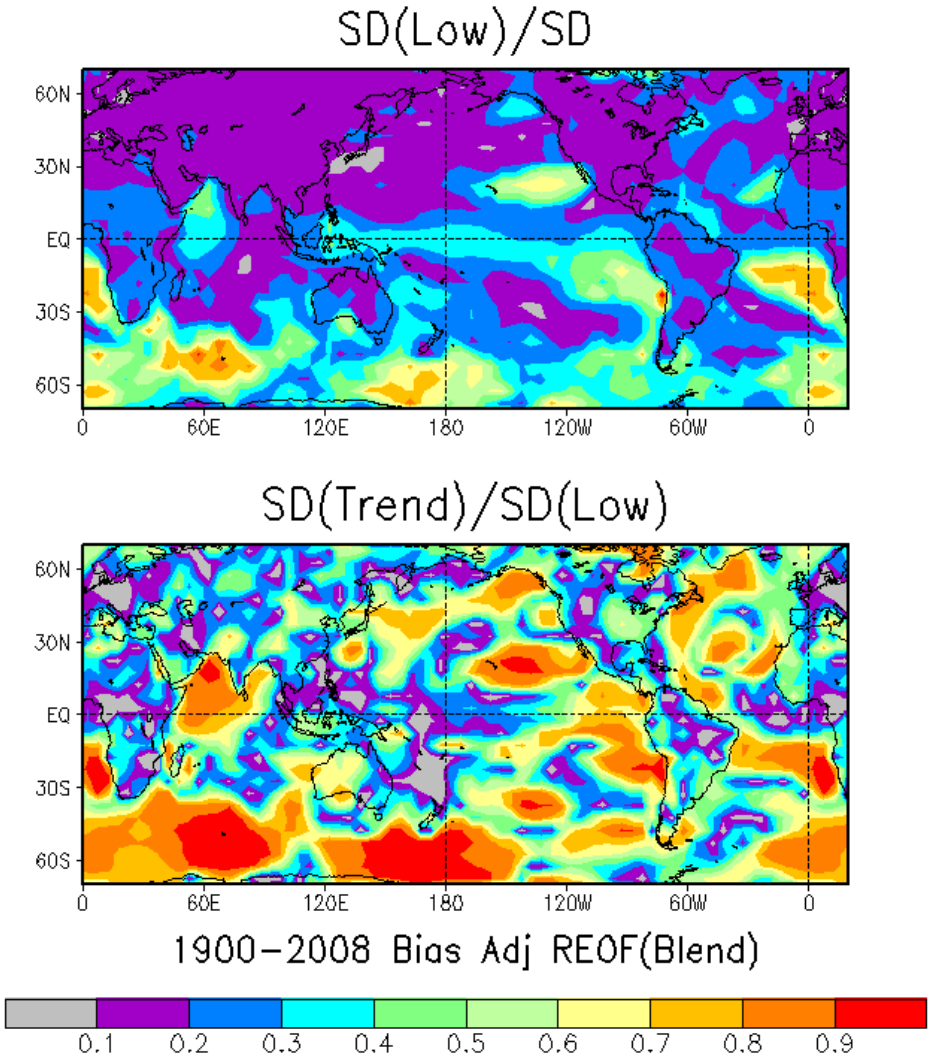

Figure 14. Ratio of low-pass filtered standard deviation to unfiltered standard deviation (upper panel) and trend standard deviation to low-pass filtered standard deviation (lower panel), all from bias adjusted REOF(Blend) monthly anomalies, 1900-2008.

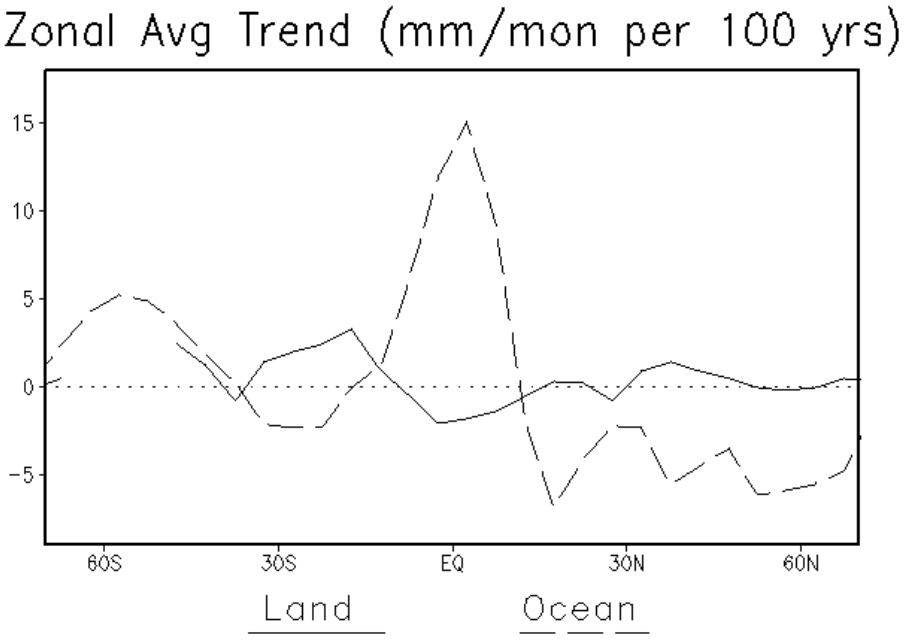

Figure 15. Zonal averages of the bias adjusted REOF(Blend) trend averaged over ocean and land areas separately.

To compare the reconstruction multi-decadal tendency with that from the AR4 model ensemble, a joint empirical orthogonal function (JEOF) analysis is done of the two fields. Both fields are low-pass filtered to concentrate on multi-decadal variations, and both are normalized so that similarities in the tendencies of both will be highlighted. About 30% of the variance is accounted for by the first JEOF mode, which shows a clear trend-like tendency with some similarities in the patterns of both fields (Fig. 16). In particular, they both indicate increasing precipitation over the Southern Ocean and in parts of the tropical Pacific. The reconstruction Southern Ocean tendency is less uniform than in the models, and the reconstruction tropical Pacific increase is shifted east relative to the models, but the similarity of these two signals suggests that the models are broadly representing multi-decadal variations in those regions.

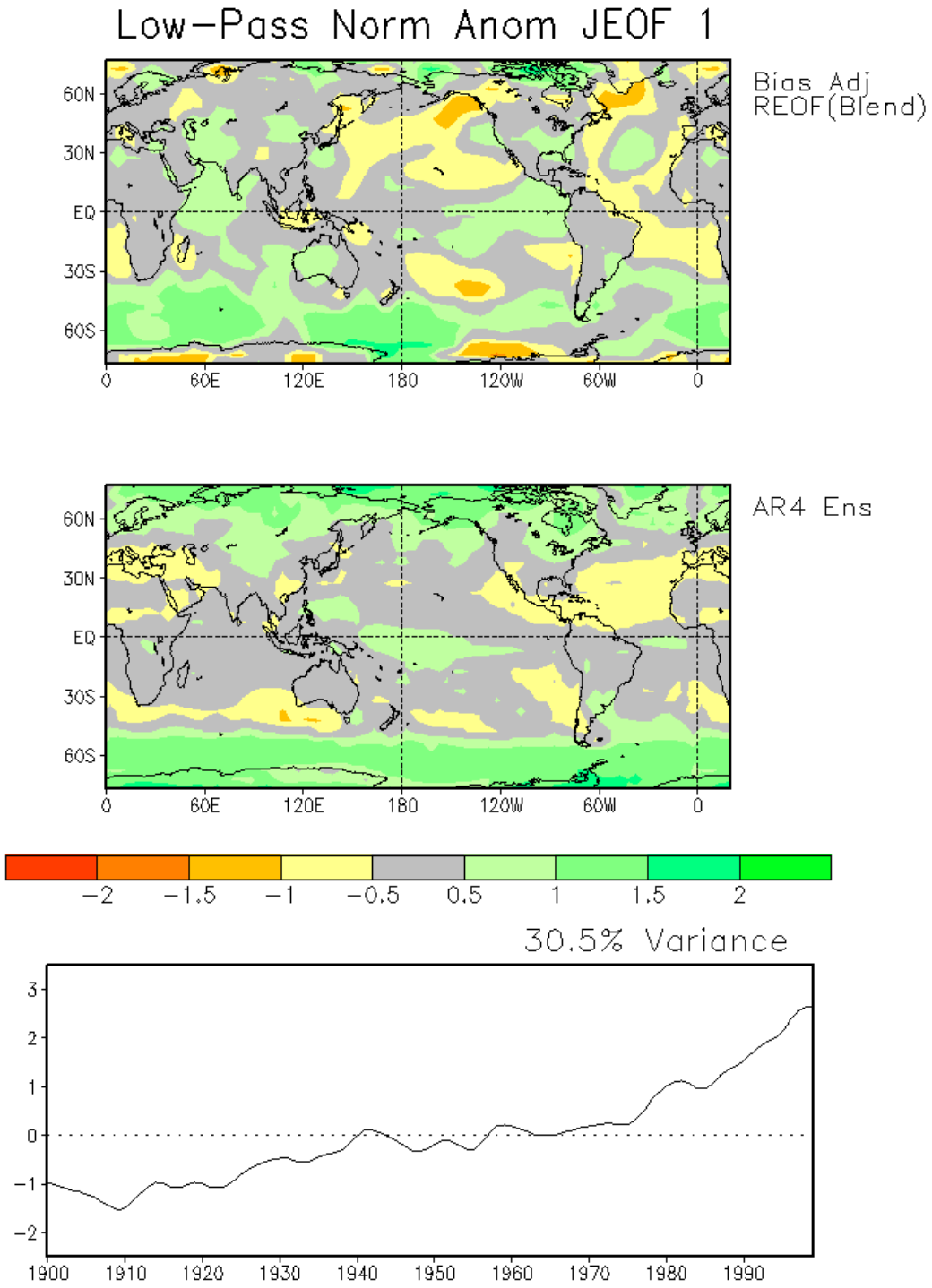

Figure 16. Joint EOF of annual low-pass filtered and normalized adjusted REOF(Blend) and AR4 model ensembles (upper 2 panels) and the associated time series for JEOF 1.

Both also show decreases in the tropical Atlantic and in some mid-latitude zones, but the similarities are not as strong in those regions. In particular, both show decreases in southern Europe, but the decrease is larger in the models and the reconstruction shows

increases in the eastern Mediterranean. Both show decreases in the Pacific near and extending into the south-west U.S. and Mexico area, but the models decrease is more extensive over land and less extensive over the North Pacific. Both show an increase over eastern North America but the models increase is further north. In addition, at high northern latitudes the model suggests more systematic increases than the reconstruction.

Here we only perform a JEOF analysis using the ensemble of models, and we do not evaluate individual models. It is possible that some models may compare with the reconstruction better in some areas than in others. Comparison of individual models is beyond the scope of this paper. Modeling groups may be able to use the reconstruction to diagnose their output over ocean and land regions over the 20th century, which could aid the development of improved coupled models.

6. Summary

Historical global precipitation has been reconstructed on a 5° monthly grid beginning 1900. Both land and ocean areas are analyzed. The land-area analysis is based on fitting the available gauge data to a set of large-scale spatial empirical analysis function (EOF) modes. That analysis, referred to as REOF, was found to be able to represent large-scale monthly variations over land. Over the oceans the REOF represents most interannual and shorter-scale variations, but because of the scarcity of gauges the multi-decadal variations over oceans were found to be less reliable. Therefore, the ocean-area analysis used is a combination of REOF with an analysis that uses a canonical correlation analysis to obtain precipitation anomalies from SST and SLP anomalies, referred to as RCCA. The combination takes the form of using the low-pass filtered RCCA to bias adjust the ocean-area low-pass REOF, forcing the ocean-area multi-decadal signal to match that of the RCCA. Both REOF and RCCA are developed using the GPCP data from 1979-2008. Statistics from that period are used to reconstruct precipitation over 1900-2008. The REOF and RCCA methods were developed and described in earlier papers. Here we show how to best combine them, and also develop uncertainty estimates for the combined reconstruction.

Evaluations of the reconstruction suggest that it should be of use for climate studies and for model evaluations. The reconstruction shows trend-like variations over both oceans and land, with the greatest changes over tropical oceans. Trends over land are weaker than over oceans, and in the tropics and sub-tropics they tend to be opposite to the ocean trends. This land-sea difference is similar to the land-sea precipitation differences associated with ENSO over the satellite period (Adler *et al.* 2008).

The reconstruction can not resolve any fine scale variations because of the filtering using spatial modes, although it should represent most large-scale variations. Because much of the reconstruction is based on a gauge data set, any systematic errors in that data set will influence the reconstruction. Most random error in the gauge data should be eliminated by filtering using a set of modes with screening of poorly sampled modes. In addition, the RCCA component of the analysis assumes that the relationships

between precipitation and the combined SST and SLP are stationary over the reconstruction period.

Error estimates take into account changes in sampling and how that affects variance, and also error estimates for the SST and SLP which may cause errors in the RCCA. However, possible errors in the gauge data set are not considered in the estimate, nor are possible errors in GPCP, or in our assumption that the relationships are stationary over the reconstruction period. In addition, errors caused by filtering the full data using the set of EOFs are also not considered here. The error estimate is a measure of how well historical data may be reconstructed relative to EOF-filtered satellite-era data.

In the future we will consider merging data from the REOF and RCCA with other data sources. Possible additional data sources include the gauge data themselves which may be re-injected to adjust the land-area analysis. In addition, data from extended model-based reanalyses may be able to improve analysis skill over both land and ocean areas (Compo *et al.* 2006). The present reconstruction is available to users at LIST WEB SITE.

ACKNOWLIDGEMENTS

We thank several centers for making their data easily available for this study, including the GHCN and SST data from the National Climatic Data Center, the GPCP from NASA, the GPCC from Deutscher Wetterdienst, the CRU analysis from Univ. East Anglia, and in addition the SLP data were supplied by the U.K. Met. Office Hadley Centre, www.metoffice.gov.uk/hadobs. This project is supported in part by the Climate Change Data and Diagnostic Program Element of the NOAA Climate Program Office and the Cooperative Institute for Climate Studies, NOAA Grant NA17EC1483. The contents of this paper are solely the opinions of the authors and do not constitute a statement of policy, decision, or position on behalf of NOAA or the U. S. Government.

REFERENCES

Adler, R.F., G.J. Huffman, A. Chang, R. Ferraro, P.-P. Xie, J. Janowiak, B. Rudolf, U. Schneider, S. Curtis, D. Bolvin, A. Gruber, J. Susskind, P. Arkin, and E. Nelkin, 2003: The version-2 Global Precipitation Climatology Project (GPCP) monthly precipitation analysis (1979-presient), *J. Hydromet.*, **4**, 1147-1167.

Adler, R. F., G. Gu, J.-J. Wang, George J. Huffman, Scott Curtis, and David Bolvin, 2008: Relationships between global precipitation and surface temperature on inter-annual and longer time scales (1979-2006). *J. Geophy. Res.*, **113**, D22104, doi:10.1029/2008JD010536.

Allan, R. J. and Ansell, T. J., 2006: A new globally complete monthly historical mean sea level pressure data set (HadSLP2): 1850-2004. *J. Climate*, **19**, 5816-5842.

Allan, R.P., and B.J. Soden, 2008: Atmospheric warming and the amplification of precipitation extremes. *Science*, **321**, 1481-1484.

Barnett, T.P., and R. Preisendorfer, 1987: Origins and levels of monthly and seasonal forecast skill for United States surface air temperatures determined by canonical correlation analysis. *Mon. Wea. Rev.*, **115**, 1825-1850.

Compo, G.P., J.S. Whitaker, and P.D. Sardeshmukh, 2006: Feasibility of a 100-year reanalysis using only surface pressure data. *Bull. Amer. Meteor. Soc.*, **87**, 175-190.

Efthymiadis, D., New, M., and Washington, R., 2005: On the reconstruction of seasonal oceanic precipitation in the presatellite era, *J. Geophys. Res.*, **110**, D06103, doi:10.1029/2004JD005339.

Held, I.M., and B.J. Soden, 2006: Robust responses of the hydrological cycle to global warming. *J. Climate*, **19**, 5686-5699.

Huffman, G.J., and Coauthors, 1997: The Global Precipitation Climatology Project (GPCP) combined precipitation datasets. *Bull. Amer. Meteor. Soc.*, **78**, 5-20.

Huffman, G.J., R.F. Adler, D.T. Bolvin, and G. Gu, 2009: Improving the global precipitation record: GPCP version 2.1. *Geophys., Res., Lett.*, **36**, L17808, doi:10.1029/2009GL040000.

Hulme, M., T.J. Osborn, and T.C. Johns, 1998: Precipitation sensitivity to global warming: Comparison of observations with HadCM2 simulations. *Geophys. Res. Letts.*, **25**, 3379-3382.

Randall, D.A., R.A. Wood, S. Bony, R. Colman, T. Fichefet, J. Fyfe, V. Kattsov, A. Pitman, J. Shukla, J. Srinivasan, R.J. Stouffer, A. Sumi and K.E. Taylor, 2007: Cilmate Models and Their Evaluation. In: *Climate Change 2007: The Physical Science Basis*. Contribution of Working Group I to the Fourth Assessment Report of the Intergovernmental Panel on Climate Change [Solomon, S., D. Qin, M. Manning, Z. Chen, M. Marquis, K.B. Averyt, M.Tignor and H.L. Miller (eds.)]. Cambridge University Press, Cambridge, United Kingdom and New York, NY, USA.

Rayner, N.A., P. Brohan, D.E. Parker, C.K. Folland, J.J. Kennedy, M. Vanicek, T.J. Ansell, and S.F.B. Tett, 2006: Improved analyses of changes and uncertainties in sea surface temperature measured in situ since the mid-nineteenth century: the HadSST2 dataset. *J. Climate*, **19**, 446-469.

Rudolf, B., 2005: Global Precipitation Analysis Products of the GPCC. DWD, Klimastatusbericht 2004, 163-170. ISSN 1437-7691, ISSN 1616-5063 (Internet www.ksb.dwd.de), ISBN 3-88148-402-7.

Sapiano, M.R.P, T.M. Smith, and P.A. Arkin, 2008: A new merged analysis of precipitation utilizing satellite and reanalysis data. *J. Geophys Res*., **113**, D22103, doi:10.1029/2008JD010310.

Schneider, U. T. Fuchs, A. Meyer-Christoffer and B. Rudolf, 2008: Global Precipitation Analysis Products of the GPCC. Global Precipitation Climatology Centre (GPCC), DWD, Internet Publikation, 1-12. (pdf 1414 KB).

Smith, T.M., and R.W. Reynolds, 2005: A global merged land air and sea surface temperature reconstruction based on historical observations (1880-1997). *J. Climate*, **18**, 2021-2036.

Smith, T.M., X. Yin, and A. Gruber, 2006: Variations in annual global precipitation (1979-2004), based on the global precipitation climatology project 2.5º analyses. *Geophys. Res. Lett.*, **33**, L06705, doi:10.1029/2005GL025393.

Smith, T.M., R.W. Reynolds, T.C. Peterson, and J. Lawrimore, 2008a: Improvements to NOAA's historical merged land-ocean surface temperature analysis (1880-2006). *J. Climate*, **21**, 2283-2296.

Smith, T. M., M. R. P. Sapiano, and P. A. Arkin, 2008b: Historical Reconstruction of Monthly Oceanic Precipitation (1900-2006), *J. Geophys. Res.*, doi:10.1029/2008JD009851

Smith, T. M., P. A. Arkin, and M. R. P. Sapiano, 2009: Reconstruction of near-global annual precipitation using correlations with SST and SLP, *J. Geophys. Res.*, (in press).

Trenberth, K.E., and J.W. Hurrell (1994) Decadal atmospheric-ocean variations in the Pacific. *Climate Dyn.*, **9**, 303-309.

Vose, R.S., T.C. Peterson, and M. Hulme, 1998: The Global Historical Climatology Network Precipitation Database: Version 2.0, In *Proceedings of the Ninth Symposium on Global Change Studies*, American Meteorological Society, Boston, Massachusetts.

Woodruff, S.D., H.F. Diaz, J.D. Elms, and S.J. Worley, 1998: COADS release 2 data and metadata enhancements for improvements of marine surface flux fields. *Phys. Chem. Earth*, **23**, 517-527.

Xie, P., and P.A. Arkin, 1996: Global monthly precipitation estimates from satellite-observed outgoing longwave radiation", *J. Climate*, **11**, 137-164.

Xie, P., and P.A. Arkin, 1997: Global precipitation: A 17-year monthly analysis based on gauge observations, satellite estimates and numerical model outputs", *Bull. Amer. Met. Soc.*, **78**, 2539-2558.

Xie, P., M. Chen, J.E. Janowiak, P.A. Arkin, and T.M. Smith, 2001: Reconstruction of the oceanic precipitation: preliminary results. Proceedings of the 26th annual Climate Diagnostics and Prediction Workshop [Copies available at http://www.cpc.ncep.noaa.gov/products/outreach/publications.shtml].

Zhang, Y., J.M. Wallace, and D.S. Battisti, 1997: ENSO-like interdecadal variability: 1900-93. *J. Climate*, **10**, 1004-1020.